J|A|C|S
ARTICLES

Published on Web 06/28/2010

Tuning the Acid/Base Properties of Nanocarbons by Functionalization via Amination

Rosa Arrigo,[†] Michael Hävecker,[†] Sabine Wrabetz,[†] Raoul Blume,[†] Martin Lerch,[‡] James McGregor,[§] Edward P. J. Parrott,[§,#] J. Axel Zeitler,[§] Lynn F. Gladden,[§] Axel Knop-Gericke,[†] Robert Schlögl,[†] and Dang Sheng Su*,[†]

Department of Anorganische Chemie, Fritz-Haber-Institut der Max-Planck Gesellschaft, Faradayweg 4-6, 14195 Berlin, Germany, Institut für Chemie der TU Berlin, Strasse des 17. Juni 135, 10623 Berlin, Germany, Department of Chemical Engineering and Biotechnology, University of Cambridge, Pembroke Street, Cambridge, CB2 3RA, United Kingdom, and Cavendish Laboratory, University of Cambridge, Cambridge, CB3 0HE, United Kingdom

Received December 9, 2009; E-mail: dangsheng@fhi-berlin.mpg.de

Abstract: The surface chemical properties and the electronic properties of vapor grown carbon nanofibers (VGCNFs) have been modified by treatment of the oxidized CNFs with NH_3. The effect of treatment temperature on the types of nitrogen functionalities introduced was evaluated by synchrotron based X-ray photoelectron spectroscopy (XPS), while the impact of the preparation methods on the surface acid−base properties was investigated by potentiometric titration, microcalorimetry, and zeta potential measurements. The impact of the N-functionalization on the electronic properties was measured by THz-Time Domain spectroscopy. The samples functionalized via amination are characterized by the coexistence of acidic and basic O and N sites. The population of O and N species is temperature dependent. In particular, at 873 K nitrogen is stabilized in substitutional positions within the graphitic structure, as heterocyclic-like moieties. The surface presents heterogeneously distributed and energetically different basic sites. A small amount of strong basic sites gives rise to a differential heat of CO_2 adsorption of 150 kJ mol^{-1}. However, when functionalization is carried out at 473 K, nitrogen moieties with basic character are introduced and the maximum heat of adsorption is significantly lower, at ∼90 kJ mol^{-1}. In the latter sample, energetically different basic sites coexist with acidic oxygen groups introduced during the oxidative step. Under these conditions, a bifunctional acidic and basic surface is obtained with high hydrophilic character. N-functionalization carried out at higher temperature changes the electronic properties of the CNFs as evaluated by THz-TDS. The functionalization procedure presented in this work allows high versatility and flexibility in tailoring the surface chemistry of nanocarbon material to specific needs. This work shows the potential of the N-containing nanocarbon materials obtained via amination in catalysis as well as electronic device materials.

1. Introduction

The chemical functionalization of nanocarbon (NC) is an essential step if such nanostructured materials are to be utilized in widespread applications. As-synthesized NCs need to be functionalized in order to improve their solubility and ease of processing.[1] Such chemical functionalization in turn influences the physicochemical properties of the NC surface. In fact, the functional groups, usually containing oxygen or nitrogen, and the delocalized electrons of the graphitic structure define the acid/base and hydrophilic/hydrophobic character of the carbon surface. These factors in turn determine the adsorption behavior and the catalytic and electrochemical properties in the bulk state. As a result, chemical functionalization can be used to tailor the surface chemical properties and the electronic properties of NC. Additionally, the functionalities on the carbon surface can be used as anchoring sites in the synthesis of carbon-based composite materials. For instance, functionalization through the grafting of organic molecules, biomolecules, or polymers onto carbon nanotubes (CNTs) is the most versatile synthetic route used to produce (bio)sensors, polymer fillers, and many other nanotube-based devices.[2]

Recently, N-containing NCs have attracted much attention in the scientific community because of their outstanding physicochemical properties.[1,3,4] Nitrogen modifies the electronic

[†] Fritz-Haber-Institut der Max-Planck Gesellschaft.
[‡] Institut für Chemie der TU Berlin.
[§] Department of Chemical Engineering and Biotechnology, University of Cambridge.
[#] Cavendish Laboratory, University of Cambridge.

(1) Chen, J.; Rao, A. M.; Lyuksyutov, S.; Itkis, M. E.; Hamon, M. A.; Hu, H.; Cohn, R. W.; Eklund, P. C.; Colbert, D. T.; Smalley, R. E.; Haddon, R. C. *J. Phys. Chem. B* **2001**, *105* (13), 2525–2528.
(2) Tasis, D.; Tagmatarchis, N.; Bianco, A.; Prato, M. *Chem. Rev* **2006**, *106* (3), 1105–1136.
(3) Terrones, M.; Jorio, A.; Endo, M.; Rao, A. M.; Kim, Y. A.; Hayashi, T.; Terrones, H.; Charlier, J. C.; Dresselhaus, G.; Dresselhaus, M. S. *Mater. Today* **2004**, *7* (10), 30–45.
(4) Czerw, R.; Terrones, M.; Charlier, J. C.; Blasé, X.; Foley, B.; Kamalakaran, R.; Grobert, N.; Terrones, H.; Tekleab, D.; Ajayan, P. M.; Blau, W.; Rühle, M.; Carroll, D. L. *Nano Lett.* **2001**, *1* (9), 457–460.

 10.1021/ja910169v

structure of the CNTs, with the effects localized at the N site[5] thereby inducing localized charge accumulation. The electronic properties of NCs are of significant interest in a variety of applications including conductive composites. The localized charge density induced by defects plays a role in electron transfer reactions[6] and facilitates the adsorption and/or dissociation of molecules, of particular importance in catalysis and sensor applications.[7]

In heterogeneous catalysis, the introduction of nitrogen in the graphitic structure of carbon materials represents a way of inducing basic surface properties. The development of new basic solid materials is a rapidly expanding area as base catalyzed reactions are of increasing interest in both academic and industrial applications.[8,9] Among these, some of the most significant are concerned with the regulation of environmental protection and sustainability in chemical processes. For example, solid basic catalysts can be used to convert biomass to biofuel[10,11] or to high value added chemicals.[12−14] More mature areas of application for basic activated carbon (AC) include fuel cells,[15] oxidation of pollutants in water,[16] and SO_2,[17−19] and NO_x abatement.[20] N-containing NCs represent potentially new catalysts for such processes.

Currently, the most commonly used synthetic route to obtain N-NC is based on the Catalytic Chemical Vapor Deposition (CCVD) of a nitrogen-containing hydrocarbon over a supported transition-metal based catalyst.[21,22] Studies reported in the literature have, however, highlighted difficulties in controlling the growth process, which very often leads to a mixture of tubes and bamboo-like[14] fibers. Despite the efforts of many investigators, the CCVD synthesis of N-CNT exhibiting a higher concentration and more uniform distribution of nitrogen sites remains a challenge. High variability in the nitrogen concentration in different tubes within the same sample batch[23] and along the cross section of one single tube[24] has been reported.

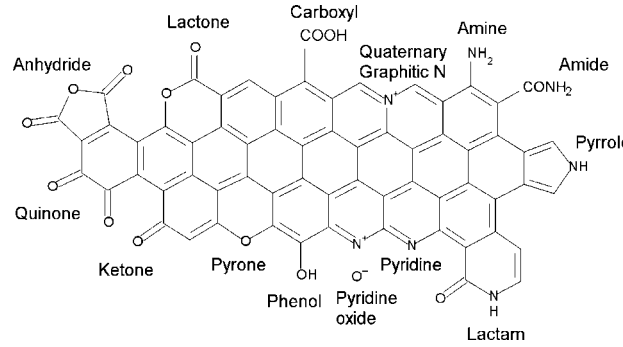

Figure 1. N and O functionalities in carbon materials.

A promising alternative synthesis route is the amination of nanostructured carbon with long chain organic amines, NH_3 or HCN. These can improve the solubility[25] and dispersion of CNTs, and introduce the desired basic moieties. Amination with NH_3 and HCN is widely used for the functionalization of activated carbon.[17,26] Considering that one-step CCVD synthesized nanostructured carbon in many cases requires treatments to disentangle formed tubes or to remove the impurities before being used,[1] such postsynthesis functionalization has distinct advantages.

Amination with NH_3 is the synthetic route chosen in this work for introducing N functionalities onto the surface of CNFs. This choice is based on the fact that such a route allows the tailoring of the surface physicochemical properties of NCs, which is an important concept for any potential application of NCs. In particular, the aim of the present work is to study the influence of the temperature of the amination treatment with NH_3 on the population of nitrogen and oxygen species and the impact of functionalization on the electronic and surface properties of the carbon materials.

As shown schematically in Figure 1, several N and O species with quite different chemical behavior may coexist on the surface of NCs. In this work, synchrotron based X-ray photoelectron spectroscopy (XPS) has been applied to determine the elemental composition and the bonding configuration of nitrogen and oxygen, respectively, on the surface of functionalized CNFs. XPS is particularly suited for the recognition of the surface species on carbon material as the measured BE shift is sensitive to the electronic structure of the photoemitting atom. Additionally, potentiometric titration, CO_2 microcalorimetry adsorption, and zeta potential measurements have been performed to characterize the acid−base properties of functionalized CNFs. HRTEM and THz-Time Domain Spectroscopy (THz-TDS) characterization have also been carried out. THz-TDS is sensitive to medium-range interactions within a material including phonon modes and intermolecular bonds, and is uniquely sensitive to electrical transport and delocalized electrons within CNT-type structures.

2. Experimental Methods

2.1. Preparation. Commercial VGCNFs were supplied by Pyrograf Products, Inc., Cedarville, OH. This material consists of

(5) Rochefort, A.; Salahub, D. R.; Avouris, P. *Chem. Phys. Lett.* **1998**, *297* (1), 45–50.
(6) Britto, P. J.; Santhanam, K. S. V.; Rubio, A.; Alonso, J. A.; Ajayan, P. M. *Adv. Mater.* **1999**, *11* (2), 154–157.
(7) Lee, C. Y.; Strano, M. S. *J. Am. Chem. Soc.* **2008**, *130* (5), 1766–1773.
(8) Fraile, J. M.; García, J. I.; Mayoral, J. A. *Catal. Today* **2000**, *57* (1−2), 3–16.
(9) Ono, Y. *J. Catal.* **2003**, *216* (1−2), 406–415.
(10) Tessonnier, J.-P.; Villa, A.; Majoulet, O.; Su, D.; Schlögl, R. *Angew. Chem. Int. Ed* **2009**, *48* (35), 6543–6546.
(11) Villa, A.; Tessonnier, J.-P.; Majoulet, O.; Su, D.; Schlögl, R. *Chem. Commun.* **2009**, *29*, 4405–4407.
(12) Matter, P. H.; Zhang, L.; Ozkan, U. S. *J. Catal.* **2006**, *239* (1), 83–96.
(13) Liu, X.; Su, D.; Schlögl, R. *Carbon* **2008**, *46* (4), 544–561.
(14) van Dommele, S.; de Jong, K. P.; Bitter, J. H. *Chem. Commun.* **2006**, *46*, 4859–4861.
(15) Strelko, V. V.; Kutsa, V. S.; Thrower, P. A. *Carbon* **2000**, *38* (10), 1499–1524.
(16) Rideal, E. R.; Wright, W. M. *J. Chem. Soc.* **1926**, *1813*, 1820.
(17) Stöhr, B.; Boehm, H. P.; Schlögl, R. *Carbon* **1991**, *29* (6), 707–720.
(18) Li, K.; Ling, L.; Lu, C.; Qiao, W.; Liu, Z.; Liu, L.; Mochida, I. *Carbon* **2001**, *39* (12), 1803–1808.
(19) Raymundo-Piñero, E.; Cazorla-Amorós, D.; Salinas-Martinez de Lecea, C.; Linares-Solano, A. *Carbon* **2000**, *38* (3), 335–344.
(20) Arenillas, A.; Rubiera, F.; Pis, J. J. *Environ. Sci. Technol.* **2002**, *36*, 5498–5503.
(21) Amadou, J.; Chizari, K.; Houllé, M.; Janowska, I.; Ersen, O.; Bégin, D.; Pham-Huu, C. *Catal. Today* **2008**, *138* (1−2), 62–68.
(22) Van Dommele, S.; Ramera-Izquirdo, A.; Brydson, R.; De Jong, K. P.; Bitter, J. H. *Carbon* **2008**, *46* (1), 138–148.
(23) Sen, R.; Satishkumar, B. C.; Govindaraj, A.; Harikumar, K. R.; Raina, G.; Zhang, J.-P.; Cheetham, A. K.; Rao, C. N. R. *Chem. Phys. Lett.* **1998**, *287* (5−6), 671–676.
(24) Terrones, M.; Kamalakaran, R.; Seeger, T.; Rühle, M. *Chem. Commun.* **2000**, *23*, 2335–2336.
(25) Basiuk, E. V.; Monroy-Pelàz, M.; Puente-Lee, I.; Basiuk, V. *Nano Lett.* **2004**, *4* (5), 863–866.
(26) Belz, T.; Bauer, A.; Find, J.; Gunter, M.; Herein, D.; Mockel, H.; Pfander, N.; Sauer, H.; Schulz, G.; Schutze, J.; Timpe, O.; Wild, U.; Schlogl, R. *Carbon* **1998**, *36* (5−6), 731–741.

Table 1. Sample Notation and Details of Corresponding Functionalization Procedure

sample	description
N-CNF473K	CNFox functionalized by NH_3 at 473 K
N-CNF673K	CNFox functionalized by NH_3 at 673 K
N-CNF873K	CNFox functionalized by NH_3 at 873 K
N-CNF873K*	CNFox annealed at 973 K in He and then in NH_3 at 873 K
CNFox	CNF functionalized by HNO_3
VGCNF	Vapor Growth Commercial Carbon Nanofiber

tubular fibers with an average diameter of 88 ± 30 nm and a specific surface area of 55 $m^2\ g^{-1}$. First, the supplied CNFs were treated with HNO_3 (Sigma-Aldrich) in order to create oxygenated functional groups that serve as reactive sites for nitrogen insertion. For this purpose, a suspension of CNFs in HNO_3 concentrate (20 g of CNT/L of HNO_3) was kept at 393 K for 2 h under continuous stirring, then rinsed with distilled water, and finally dried at 383 K for several hours. Through oxidation treatments, the removal of the accessible metal impurities occurs. Aminated samples were then obtained through thermal treatment of the preoxidized CNFs (10 g for each batch) with NH_3 in the temperature range 473−873 K for 4 h. Furthermore, amination at 473 K has been performed on oxidized CNF pretreated by annealing in He up to 973 K for 2 h to gain detailed information about the role of the oxygen functionalities on the surface of CNFs. In the following, the sample notation as reported in Table 1 will be used.

2.2. Characterization Techniques. X-ray photoelectron spectroscopy (XPS) has been performed at the synchrotron radiation facility BESSY II using monochromatic radiation of the ISISS beamline as a tunable X-ray source.[27] XP spectra were obtained in ultra high vacuum using the end-station designed and constructed at the FHI. Details of the setup are described elsewhere.[28] The O1s, N1s envelopes were fitted using mixed Gaussian−Lorentzian component profiles after subtraction of a Shirley background[29] using Casa XPS software.[30] In spectra in which the species abundance was close to the detection limit, a linear background has been subtracted. The numbers of peaks introduced have been determined by applying the difference method[31,32] to spectra recorded sequentially during temperature programmed XPS experiments.[33] The fitting was performed by fixing the peak maximum within ±0.1 eV for all spectra and applying a full width half-maximum (fwhm) of 1.4 −1.6 eV. The excitation energy for C1s/N1s/O1s core level spectra were 435/550/680 eV, respectively, resulting in a high surface sensitivity with an inelastic mean free path (IMFP) of the photoelectrons of about 0.86 nm. The spectra have been normalized to the impinging photon flux that has been determined by a cleaned Au foil and corrected for the fraction of higher order and the electron current in the storage ring. Quantitative XPS data analysis was performed using theoretical cross sections.[34] Overall nitrogen and oxygen contents were determined using a LECO TC-300/EF-300 N/O analyzer (hot gas extraction). After thermal decomposition of the samples in a Ni/Sn/Pt-melt at ∼3000 K under helium atmosphere (graphite-heated resistance furnace, graphite crucible), the oxygen content was determined by measurement of the CO_2 concentration (after oxidation of CO) with an IR-cell. Analysis of the nitrogen concentration was carried out by measuring the thermal conductivity of the helium/nitrogen mixture after absorption of CO_2. The accuracy is ∼2% of the N/O present.

THz-TD spectroscopy has been carried out as previously reported for unfunctionalized NCs.[35,36] Briefly, subpicosecond coherent pulses of broadband terahertz radiation (0.1−4 THz) were generated by photoexcitation of a DC-biased semi-insulating GaAs substrate by 12 fs pulses of a near-infrared (NIR) laser (Femtolasers, Femtosource cM1, Vienna, Austria, center wavelength 800 nm). The pulsed terahertz radiation was transmitted through the CNF sample material and detected using electro-optic sampling with a ZnTe crystal.

Potentiometric titration of the basic sites was carried out on the samples using a Mettler Toledo Titrator. Approximately 0.2 g of sample was suspended in 50 mL of KCl 1×10^{-3} M, sonicated and equilibrated for several hours. Prior to each measurement, the suspension was continuously saturated with Argon to eliminate the influence of CO_2 until the pH was constant. Volumetric standard of HCl (0.01M) was used as titrant, starting from the initial pH of the CNFs suspension. The pK_a value is calculated as the pH at a volume of titrant added corresponding to half the volume at the equivalent point (EQP). To obtain information about the surface charge of N-CNFs, zeta potential measurements were performed using a Malvern Zetasizer. Approximately 5 mg of CNFs was dispersed in 50 mL of $NaClO_4$ and sonicated for 10 min. Thereafter, the suspensions were kept at 25 °C and the pH was adjusted to a value of 12 using 0.1 M sodium hydroxide. A titration was performed from pH 12 to pH 2 by adding 0.1 M hydrochloric acid and the zeta potential was recorded as function of pH.

For calorimetric measurements, a Calvet calorimeter (MS70 SETARAM) has been combined with a house-designed high vacuum system, which enables the dosage of probe molecules within a range of 0.02 μmol. The pressure-controlled dosing systems with calibrated volume allows for the detection of the amount of adsorbed molecules (adsorption isotherm) as well as differential heat of adsorption and gives the possibility to elucidate the distribution of the adsorption sites along the range of adsorption heats.[37] The samples were pretreated and activated under mild conditions to minimize thermal and mechanical stress. All samples were pressed under low pressures (125 MPa) and cut into small pellets, which were sieved to a diameter of 0.4−0.6 mm. The activation was conducted separately in the calorimetric cell connected to a turbomolecular-pump (Balzers). The activation was performed for 17 h at 373 K with a heating rate of 2 K min^{-1}. The final pressure in the degassed cell was approximately 10^{-6} mbar. The cell was cooled to room temperature, placed inside the calorimeter, and connected to the microcalorimetric gas-adsorption system. Subsequently, CO_2 was dosed stepwise at 313 K. Pressure (mbar), adsorption temperature (°C) and the heat signal (V) were recorded. We have adopted the calorimetric sign criterion (positive energetic quantity for an exothermic process).

3. Results

The results of the characterization of the samples through the various techniques employed is presented and discussed with the aim to analyze the influence of treatment temperature on the distribution of nitrogen and oxygen functionalities and the impact of the thermal treatment in NH_3 on the physicochemical properties of VGCNFs.

3.1. XPS Characterization. XPS data provide information on the graphitic order of the CNFs and the chemical nature of the

(27) Hävecker, M.; Senf, F.; Eberhardt, W.; Schlögl, R., in preparation.
(28) Vass, E. M.; Hävecker, M.; Zafeiratos, S.; Teschner, D.; Knop-Gericke, A.; Schlögl, R. *J. Phys.: Condens. Matter* **2008**, *20* (18), 184016–29.
(29) Shirley, D. A. *Phys. Rev. B: Solid State* **1972**, *5*, 4709–4714.
(30) Fairley, N.; Carrick, A. *The Casa Cookbook*; Acolyte Science: Cheshire, U.K., 2005.
(31) Proctor, A.; Sherwood, P. M. A. *J. Electron Spectrosc. Relat. Phenom.* **1982**, *27* (1), 39–56.
(32) Proctor, A.; Sherwood, P. M. A. *Anal. Chem.* **1982**, *54*, 13–19.
(33) Arrigo, R.; Hävecker, M.; Schlögl, R.; Su, D. *Chem. Commun.* **2008**, *40*, 4891–4893.
(34) Yeh, J. J.; Lindau, I. *At. Data Nucl. Data Tables* **1985**, *32*, 1–155.
(35) Parrott, E. P. J.; Zeitler, J. A.; McGregor, J.; Oei, S. P.; Unalan, H. E.; Tan, S. C.; Milne, W. I.; Pepper, M.; Tessonnier, J. P.; Schlögl, R.; Gladden, L. F. *J. Phys. Chem. C* **2009**, *113* (24)), 10554–10559.
(36) McGregor, J.; Huang, Z.; Parrott, E. P. J.; Zeitler, J. A.; Nguyen, K. L.; Rawson, J. M.; Carley, A.; Hansen, T. W.; Tessonnier, J.-P.; Su, D. S.; Teschner, D.; Vass, E. M.; Knop-Gericke, A.; Schlögl, R.; Gladden, L. F. *J. Catal.* **2010**, *269* (2), 329–339.
(37) Coker, E. N.; Jia, C. J.; Karge, H. G. *Langmuir* **2000**, *16*, 1205–1210.

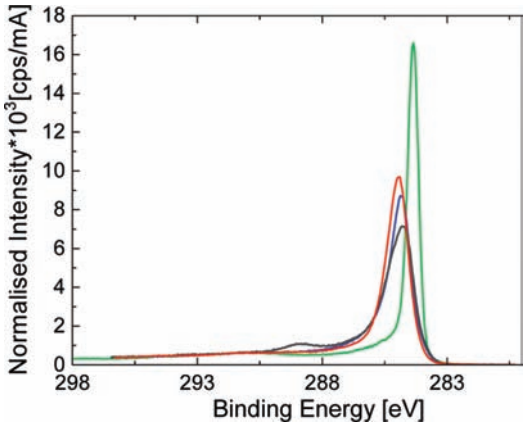

Figure 2. C1s spectra for the CNF sample and for HOPG reference: HOPG (green line); N-CNF873K (blue line); CNFox (black line); VGCNF (red line).

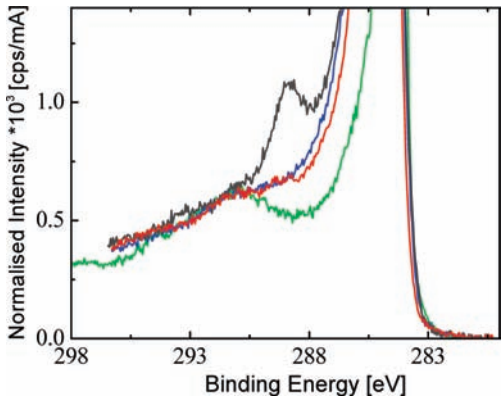

Figure 3. Detail on higher BE region of the C1s spectra: HOPG (green line); N-CNF873K (blue line); CNFox (black line); VGCNF (red line).

functional groups through analysis of the C1s and of the N1s and O1s XP spectra, respectively.

To analyze the C1s spectra of CNFs, rather than searching for a suitable fitting model, it is convenient to refer the corresponding spectra to the HOPG reference (Figures 2 and 3). This approach gives a qualitative insight in the structural feature of pristine and functionalized CNFs. Figure 2 shows the C1s spectra for the samples investigated and also of HOPG after annealing at 873 K as a reference. The thermal treatment was performed on HOPG with the aim of cleaning the surface of any trace of impurities. In this way, the C1s line shape of almost pure, defect-free graphite can be obtained as standard for which the line width is mainly determined by the spectral resolution.[38]

The spectra have been normalized with the shakeup at 290.9 eV, assuming that this feature is present in carbon materials which contain, in part, carbon with a comparable degree of graphitic order. Such a normalization approach highlights differences in the C1s peak shape which are directly related to the CNF structure. In fact, for all samples, the observed intensity of the maximum of the C1s peak is lower than that of HOPG, with the N functionalized (N-CNF873K) and the O functionalized (CNFox) samples having a lower intensity than unfunctionalized VGCNF. Furthermore, the apparent binding energy (BE) of the main peak differs slightly between different samples: 284.4 eV for HOPG; 284.7 eV for CNFox; 284.8 eV for N-CNF873K, and 284.9 eV for VGCNF.

(38) Prince, K. C.; Ulrych, I.; Peloi, M.; Ressel, B.; Cháb, V.; Crotti, C.; Comicioli, C. *Phys. Rev. B* **2000**, *62* (11), 6866–6868.

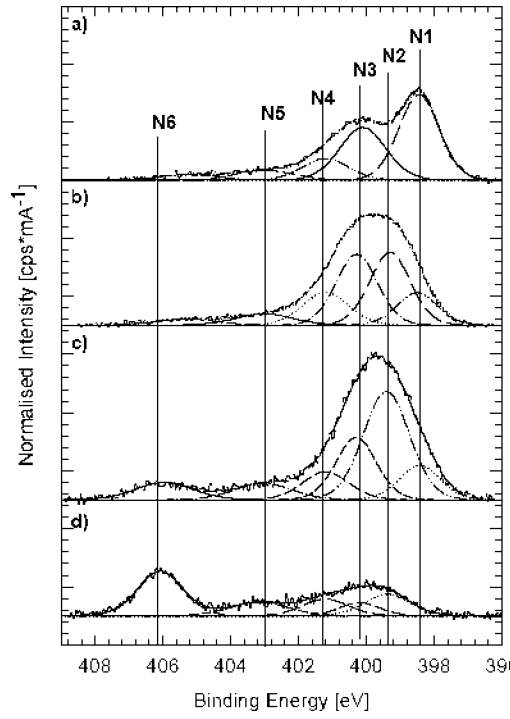

Figure 4. XP N1s spectra of (a) N-CNF873K; (b) N-CNF673K; (c) N-CNF473K; (d) CNFox.

Compared to HOPG, these shifts, together with a broadening on the high BE side, strongly suggest the presence of additional components, vide infra.

In Figure 3, details of the high-energy region of the C1s spectra are presented. The difference spectra of the C1s for the functionalized samples with respect to HOPG after normalization with shakeup at 290.9 eV are reported in Figure S1 (Supporting Information). With respect to HOPG, all samples exhibit a region of high intensity between ~285 and ~291 eV. In particular, in the case of CNFox, a distinct additional feature at ~288.8 eV is observed.

Oxygen and nitrogen moieties introduced through functionalization can be analyzed by the O1s and N1s emissions, respectively. As described above, a multitude of species coexist with similar BE shifts in the C1s XP spectrum. This is also encountered in the N1s and O1s regions. Because of the large intrinsic peak line-width, the various peaks overlap with each other giving rise to broad, unresolved peaks. In case of very broad peaks, a mathematical analysis of the XPS data, for example, derivative or difference spectra method,[31,32] can be used to determine the appropriate number of peaks to fit to the XP spectrum.

In our recent work,[33] we demonstrated the possibility to experimentally establish by means of temperature programmed XPS combined with on-line MS the number of different species of nitrogen that are present on the surface of NH_3 treated CNFs. Similarly, in the present work, the difference method was applied to all of the spectra recorded during temperature programmed XPS measurements. As such, it was possible to identify the number of peaks, peak shape, and fwhm.[39]

According to the difference spectra analysis method, six components are present in the N1s spectrum. The binding energies (eV) are as follows: N1, 398.4 ± 0.1; N2, 399.5 ± 0.1; N3, 400.1 ± 0.1; N4, 401.1 ± 0. 1; N5, 403 ± 0.1; N6, 406 ± 0.1. The XP O1s core level spectra have been deconvoluted by introduction of five contributions with peak maxima as follows: O1, 530.7 ± 0.1; O2, 531.4 ± 0.1; O3, 532.4 ± 0.1; O4, 533.7 ± 0.1; O5, 535 ± 0.1. The deconvoluted XP N1s and O1s core level spectra for all samples are shown in Figures 4 and 5, respectively. Depending

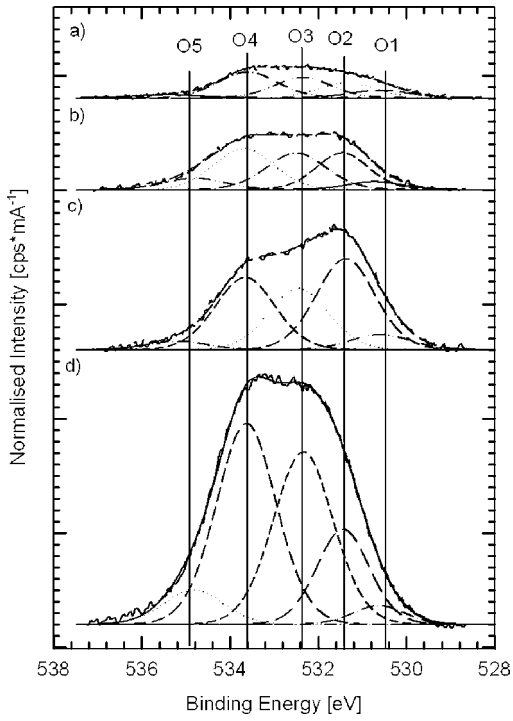

Figure 5. XP O1s spectra of (a) N-CNF873K; (b) N-CNF673K; (c) N-CNF473K; (d) CNFox.

on the treatment temperature, different overall N1s and O1s peak line shapes were observed reflecting a different distribution of N and O species.

To highlight the change in the distribution of N and O species with increasing temperature of functionalization, the abundance of all N and O components for the series of samples investigated has been calculated and is shown in Table 2 alongside their corresponding BE.

From the data shown in Table 2, it is clear that the amount of the N1 species increases with the functionalization temperature and it is the most abundant species for the sample functionalized at 873 K. In contrast, N2 is the main species when the functionalization is conducted at lower temperature (473 K). Considering that the N insertion occurs through the reaction of NH_3 with the oxygenated species on the surface, and that the total amount O and N for this sample is similar (abundance of N and O in Table 2), it is quite probably that N is present within functionalities which also contain O.

When the functionalization is conducted at 673 K, the N1s line shape is less defined, with broadening to the high BE side. This can be explained by the simultaneous decrease of N2 and the increase of N3 nitrogen. The intensity of the N3 species is greatest for N-CNF673K, decreasing for the sample functionalized at higher temperature. As we reported previously,[33] N3 species are converted to N1 species with increasing temperature. The similar O and N content in the sample N-CNF673K suggests that again for this sample nitrogen is present in functionalities accompanied by oxygen. The amination process, in general, produces a strong decrease in the absolute abundance of the carbon−oxygen groups (O4 and O3).

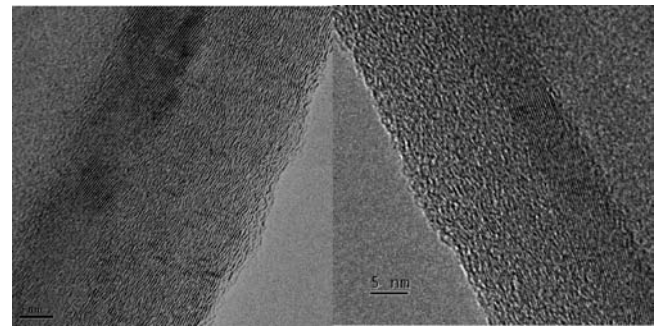

Figure 6. HRTEM images of CNF before (left side picture) and after (right side picture) NH_3 functionalization.

In the case of CNFox, N6 is the main species present in the nitrogen spectra of the oxidized CNFs. A further very broad peak is present between 398 and 400 eV with its maximum at 399.6 eV for CNFox. It should be mentioned that the N2 species is located at 399.6 eV for the CNFox and at 399.4 eV for the other samples (N-CNF473K, N-CNF673K, N-CNF873K). This implies that the N2 species in the CNFox has a different chemical structure than in the aminated samples. The structure of the functional groups is discussed in detail in section 4.

3.2. Other Techniques. In addition to XPS characterization of the samples, additional measurements have been carried out to provide complementary information. It is through the combination of the various techniques employed that a complete understanding of the effects of amination can be established. TEM and hot-gas extraction provide structural information and overall elemental composition, respectively; potentiometric titration, zeta potential, and microcalorimetry measurements provide insights into the nature of the surface sites present, while THz-TDS characterizes the electronic structure of the CNFs.

3.2.1. Structural Studies. TEM images of the CNFs before (left) and after amination at 873 K (right) are shown in Figure 6. These studies show that the CNFs under investigation are characterized by comparatively thick walls, composed of two parts with differing graphitic order: an inner layer comprising a highly graphitized structure with a thick layer of pyrolytic carbon on the external side. As Figure 6 shows, the functionalization treatment with NH_3 does not produce substantial modification of the structure of the CNFs.

While the structure as revealed by TEM shows relatively little change upon amination, the chemical composition of the sample does alter. The elemental composition of the samples has been evaluated by two techniques: XPS (see section 3.1) and hot-gas extraction. The results of these analyses are shown in Table 3. XPS is a surface sensitive technique, and hence, the values determined by XPS represent the surface composition. In contrast, hot-gas extraction provides the bulk elemental composition. Both of these parameters are important with, for

Table 2. Summary of XPS Data[a]

sample	N1 (398.4)	N2 (399.4)	N3 (400.1)	N4 (401.1)	N5 (403)	N6 (406)	O1 (530.7)	O2 (531.4)	O3 (532.4)	O4 (533.7)	O5 (535)
CNFox	0	1.3	0.5	0.7	0.8	2	0.8	3.8	8	9.2	1.6
N-CNF473	1.4	5	2.5	1.3	1	1	0.7	4.2	2.9	3.4	0.4
N-CNF673	1.6	6.7	5.4	2.8	1.2	1	0.6	2.9	3.3	3.8	1
N-CNF873	3.5	0	2.5	1	0.6	0.4	0.4	0.7	1	1.2	0.1

[a] Species abundance is given in atom percentage; in parentheses, the corresponding binding energies (eV) ±0.1 eV.

Table 3. Elemental Composition As Determined by XPS and Hot Gas Extraction

	N (at%)		O (at%)	
sample	surface (5−10 Å)[a]	bulk[b]	surface[a]	bulk[b]
N-CNF473K	12.3	1.3	11.7	2.2
N-CNF673K	18.8	1.5	11.7	1.2
N-CNF873K	8	1.1	3.4	0.7
N-CNF873K*	3	-	19	-
CNFox	5	0.6	23.3	5.6
VGCNF	1.3		6.7	

[a] Determined by XPS. [b] Determined by hot gas extraction.

example, surface composition crucial in sensor applications but bulk structure of greater relevance in, for example, composite materials. It is clear from Table 3 that the nitrogen and oxygen groups are preferentially located at the surface of the NCs. Additionally, only those samples with acidic oxygen functionalities present prior to amination (N-CNF473K, N-CNF673K, and N-CNF873K) show high levels of nitrogen incorporation as a result of functionalization with NH_3. The thermal decomposition of these oxygen functionalities, with thermal stability below 973 K, results in a considerable decrease in the amount of nitrogen covalently bonded to the CNFs surface (sample N-CNF873K*).

3.2.2. Nature of Surface Sites. The chemical nature of the surface sites created as a result of functionalization has been investigated by potentiometric titration, zeta potential, and microcalorimetric measurements. These data provide a direct indication of the nature of the surface, for example, by providing a description of the number and strength of basic sites present: these are the sites which interact with adsorbates in sensor and catalytic applications.

Figure 7 shows the results of potentiometric titration of the basic sites by HCl for N-CNF473K, N-CNF673K, and N-CNF873K. The titration curves are characterized by two distinct equivalent points (EQP). The pK_a values of the two species corresponding to the two EQP are numerically determined by considering the pH value at half of the volume of titrant added to the EQP. At this point, the pH of the suspension corresponds to the pK_a of the basic site titrated.

The amount of basic sites is of the same order for all samples, with slightly stronger basic character for the samples functionalized at higher temperatures (higher pK_a value). Titration data show excellent agreement with zeta potential measurements as shown in Figure 8. The zeta potential of the CNFox is negative over the whole pH range investigated because it contains mainly acidic groups. The pH at which the surface charge approaches zero shifts to higher values with increasing functionalization temperature. NH_3 functionalization shifts the isoelectric point to higher pH as the result of the introduction of basic sites.

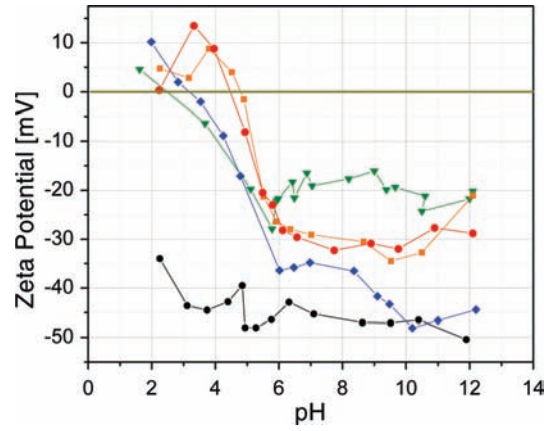

Figure 8. Zeta potential data: (green triangles) CNF, (black rhombus) CNFox, (blue rhombus) N-CNF473K, (orange squares) N-CNF673K, (red circles) N-CNF873K.

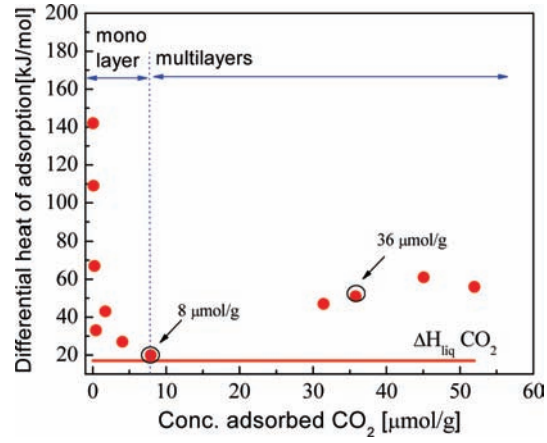

Figure 9. Differential heat of CO_2 adsorption for N-CNF873K.

To further determine the number and the strength of the basic sites, the adsorption of carbon dioxide was studied by microcalorimetry at 313 K. The differential heat of adsorption as a function of the CO_2 uptake for the sample N-CNF873K is reported in Figure 9. At low CO_2 coverage, the initial differential heat of adsorption is very high and decreases rapidly to reach a plateau with increasing CO_2 pressure. The high values for the initial heat of adsorption and the rapid decrease with increasing coverage demonstrate the presence of heterogeneously distributed and energetically different (basic) adsorption sites. Above 8 μmol g^{-1} of CO_2, the differential heat of adsorption reaches the value of the heat of condensation of CO_2 (-17 kJ mol^{-1}) indicating that in this range the monolayer is completed and multilayer adsorption proceeds. Successively, at higher coverage of CO_2, the heat of adsorption increases again

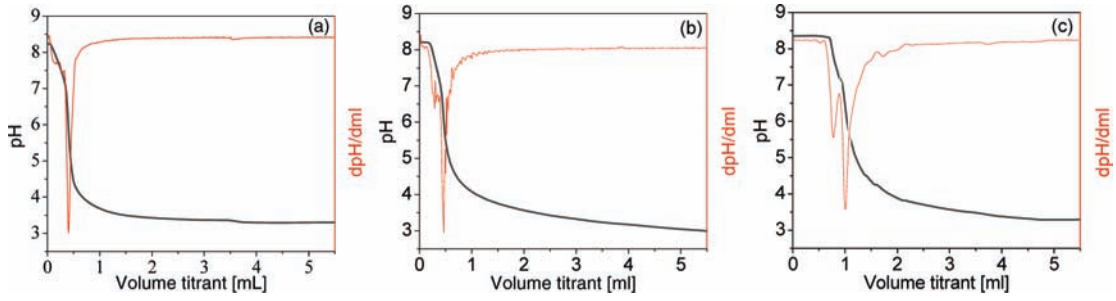

Figure 7. HCl titration curve (black) and first derivative (red): (a) N-CNF473K; (b) N-CNF673K; (c) N-CNF873K.

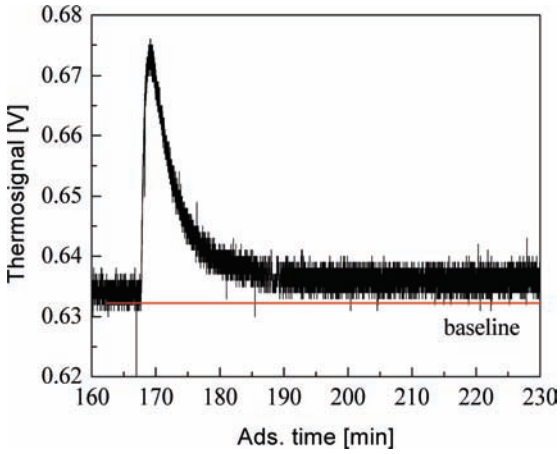

Figure 10. Integral heat signal vs time at 1.7 μmol g^{-1} of CO_2 (monolayer region) for N-CNF873K.

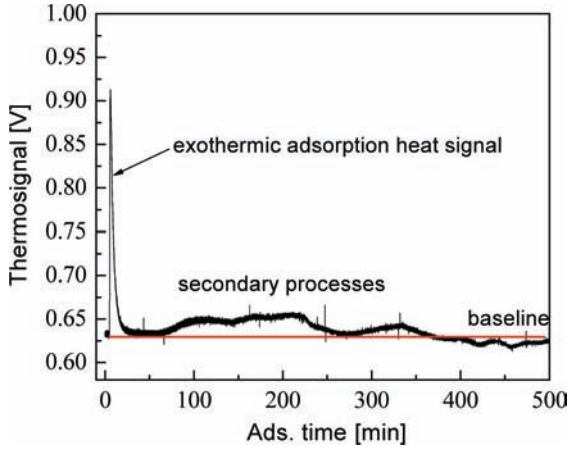

Figure 11. Integral heat signal vs time at 36 μmol g^{-1} of CO_2 (multilayer region) for N-CNF873K.

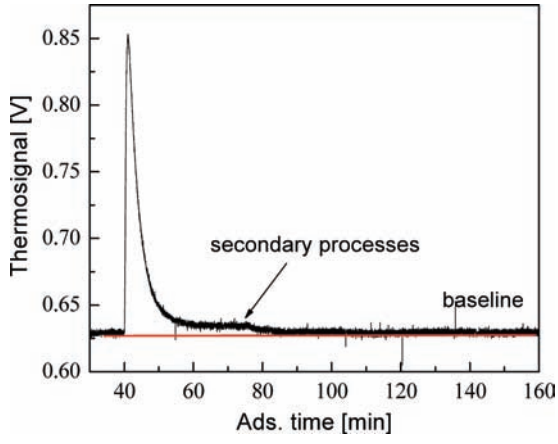

Figure 12. Integral heat signal vs time at 45 μmol g^{-1} (multilayer region) of CO_2 for N-CNF873K.

indicating that the adsorption of CO_2 is accompanied by secondary exothermic processes.

This can be better observed in the integral heat of adsorption recorded as function of time reported for N-CNF873K in Figures 10−12. Figure 10 shows the heat signal at low CO_2 coverage (1.7 μmol g^{-1}) corresponding to a differential heat of adsorption of 100 kJ mol^{-1} (Figure 9). After the adsorption peak, the heat signal reaches the baseline which is an indication of a "quasi-pure" adsorption process.

With increasing CO_2 coverage (36 μmol g^{-1}), a differential heat of adsorption of 51 kJ mol^{-1} is observed (Figure 9 multilayer region). After the adsorption peak (Figure 11), the heat signal again reaches the baseline. However, after a certain time, exothermic secondary processes occur as suggested by the increase of the heat signal in Figure 11. At still higher CO_2 coverage (45 μmol g^{-1}), the differential heat of adsorption is 61 kJ mol^{-1} (Figure 9). Here the integral heat signal after the adsorption peak does not reach the baseline and at this condition the secondary processes occur earlier (Figure 12). For N-CNF873K, the total integral heat of adsorption measured (−575 mJ) is much higher than the integral heat of desorption (+138 mJ), indicating the irreversibility of those secondary processes. The secondary process occurs at lower pressure for the samples N-CNF673K and N-CNF473K indicating a higher reactivity toward CO_2 for these samples (Figure 13).

The CO_2 adsorption isotherms of the samples investigated are reported in Figure 14. The monolayer is completed at <2 mbar CO_2 for N-CNF873K and <6 mbar for N-CNF473K: above this value, multilayer adsorption occurs (e.g., identified by a frame in Figure 14). It is in the multilayer region that secondary reactions occur. Among the samples investigated, only N-CNF873K adsorbs a considerable amount of CO_2, indicating a high quantity of basic sites. For all other samples, the number of basic sites is very low. As the monolayer is formed before secondary reactions take place over N-CNF473K and N-CNF873K, the amount of CO_2 adsorbed up to this point is indicative of the number of adsorption sites present on the sample. For the other samples, because secondary reactions occur before monolayer formation, the quantification of the basic sites cannot be entirely accurate. It is also possible to calculate the specific surface area of the samples from CO_2 adsorption data. The surface area calculated from CO_2 adsorption applying the Langmuir adsorption model is 2 and 1 m^2 g^{-1} for N-CNF873K and N-CNF473K, respectively. This value differs significantly from the one calculated on the basis of N_2 adsorption which was ∼55 m^2 g^{-1}.

3.2.3. Electronic Characterization. As is evidenced by the above methods, nitrogen functionalization alters the electronic properties of the starting CNFs. To further investigate these changes, THz-TDS has been employed. THz-TDS provides information on the bulk electronic system of the nanofibers and has recently been employed to characterize the electronic properties of NCs with the measured parameters correlated with catalytic performance and applications in composite materials.[35,36] Significantly, during measurement the samples are not in suspension, nor are the measurements conducted on single fibers but on aggregates. Furthermore, the technique is noncontact and nondestructive. The results are hence directly applicable to applications such as catalysis and sensor devices. Figure 15 shows the measured absorption coefficient, refractive index, and the real and imaginary components of conductivity. As can be seen in Figure 15, there are some clear differences in the terahertz characteristics of the CNF before and after functionalization. Following previous work,[35,36] we have attempted to determine the electrical characteristics of the materials by modeling the dielectric response of the CNT films using a Drude-Lorentz (DL) model and employing an effective medium approximation (EMA). In this way, it is possible to extract parameters characterizing the electronic landscape of the samples. The results of these fits are described in section 4.3.

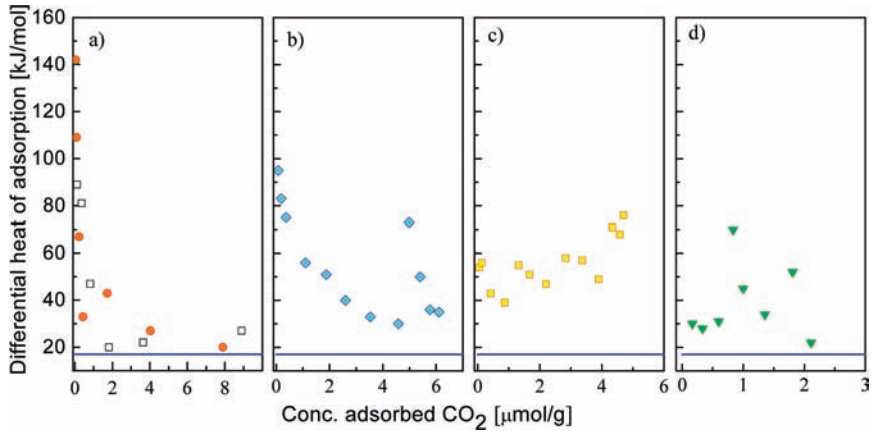

Figure 13. Differential heat of CO_2 adsorption versus amount of CO_2 uptake in the monolayer region for the CNF samples: (a) N-CNF873K: first adsorption (red scatters); readsorption (black-white scatters); (b) N-CNF473K (blue scatters); (c) N-CNF673K (yellow scatters); (d) VGCNF (green scatters); ΔH_{liq} CO_2 (blue line).

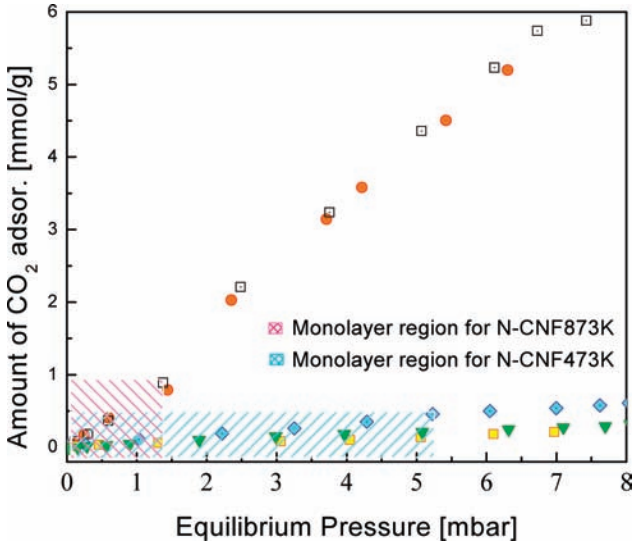

Figure 14. CO_2 adsorption isotherms: first adsorption on N-CNF873K (red circles); readsorption on N-CNF873K (black-white squares); N-CNF473K (blue rhombus); N-CNF673K (yellow squares); VGCNF (green triangles).

4. Discussion

In this work, amination has been carried out on previously oxidized CNFs with the aim to introduce surface N species. Different N and O functionalities with quite different properties have been reported on carbon[40] and are illustrated schematically in Figure 1. To identify the species created through functionalization in the present work, XPS studies have been conducted as reported in section 3.1. The XP spectra reported are highly complex and are not straightforward to interpret. To this end, a detailed description of the assignment of XPS peaks and the rationale behind this assignment is provided in section 4.1. This determination of the surface functionalities present allows for a detailed description of the surface structure of the CNFs after amination (section 4.2), while section 4.3 describes the bulk properties of the materials.

4.1. Assignment of XPS Peaks. 4.1.1. C1s Region. Useful information regarding the structural modification of the CNFs subjected to the functionalization treatments can be extracted from the C1s spectra. The effect of functionalization on the C1s spectrum has been extensively studied in the fields of polymer[41] and graphite fiber science.[31,32,42−45] Although the fitting parameters have not yet been unanimously settled on, it is generally accepted in the literature that the main feature in the C1s spectrum of carbon materials is an asymmetric peak attributed to sp^2 carbon atoms in a graphitic structure. The asymmetry to the high binding energy (BE) side of the C1s peak of defect-free graphite is associated with the excitation of conduction electrons, which occurs in metal or semimetals as a consequence of the relaxation of the core-hole generated by the primary photoemission process.[46,47] The peak line shape for defect-free graphite is represented here by the photoemission spectra recorded for HOPG (Figure 2). The BE of this peak may vary within a few tenths electronvolts: the value reported for HOPG varies between 284.6 eV[42,48,49] and 284.4 eV.[50] The peak line shape is well described by the Doniach-Sunjic function; however, the asymmetry factor depends on the extent of defects within the structure. Investigations on the effect of ion bombardment on the C1s spectrum of HOPG have highlighted a decrease in both intensity and the asymmetry factor.[51] Accordingly, the observed high intensity contribution with its maximum at around 285 eV is attributed to sp^2 or sp^3 carbon species, associated with defects in the graphitic structure and thus not present in the HOPG spectrum. With respect to HOPG, the CNF samples

(39) Arrigo, R.; Hävecker, M.; Blume, R.; Knop-Gericke, A.; Su, D.; Schlögl, R., in preparation.
(40) Radovic, L. R.; Silva, I. F.; Ume, J. I.; Menéndez, J. A.; Leon, C. A.; Leon, Y.; Scaroni, A. W. *Carbon* **1997**, *35* (9), 1339–1348.
(41) Clark, D. T.; Thomas, H. R. *J. Polym. Sci., Polym. Chem. Ed.* **1978**, *16*, 791–820.
(42) Lahaye, J.; Nanse, G.; Fioux, P.; Bagreev, A.; Broshnik, A.; Strelko, V. *Appl. Sur. Sci.* **1999**, *147* (1−4), 153–174.
(43) Sherwood, P. M. A. *J. Electron Spectrosc. Relat. Phenom.* **1996**, *81* (3), 319–342.
(44) Keller, N.; Maksimova, N. I.; Roddatis, V. V.; Schur, M.; Mestl, G.; Butenko, Y. V.; Kuznetsov, V. L.; Schlögl, R. *Angew. Chem., Int. Ed.* **2002**, *41*, 1885–1888.
(45) Desimoni, E.; Casella, G. I.; Cataldi, T. R. I.; Salvi, A. M.; Rotunno, T.; Di Croce, E. *Surf. Interface Anal.* **1992**, *18* (8), 623–630.
(46) Van Attekum, P. M. Th. M.; Wertheim, G. K. *Phys. Rew. Lett.* **1979**, *43* (25), 1896–1898.
(47) Speranza, G.; Minati, L. *Surf. Sci.* **2006**, *600* (19), 4438–4444.
(48) Werner, H.; Herein, D.; Blöcker, J.; Henschke, B.; Tegtmeyer, U.; Schedel-Niedrig, Th.; Keil, M.; Bradshaw, A. M.; Schlögl, R. *Chem. Phys. Lett.* **1992**, *194* (1−2), 62–66.
(49) Atamny, F.; Blöcker, J.; Henschke, B.; Schlögl, R.; Schedel-Niedrig, T.; Keil, M.; Bradshaw, A. M. *J. Phys. Chem.* **1992**, *96* (11), 4522–4526.
(50) Müller, J.-O. Ph.D. Thesis, Fritz-Haber-Institut der MPG, Berlin, 2005, p 69.
(51) Yang, D.-G.; Sacher, E. *Surf. Sci.* **2002**, *504*, 125–137.

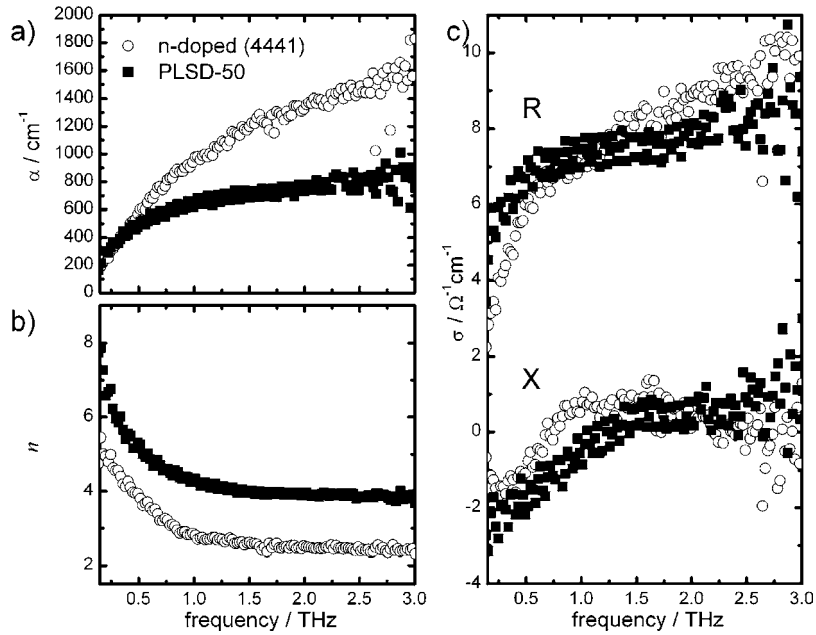

Figure 15. Absorption coefficient (a), real refractive index averaged from multiple measurements (b), and conductivity (c) real (R) and imaginary (X) components of the VGCNFs (■) and NCNF873K (○) samples at terahertz frequencies.

in the present study exhibit a less intense, broader, and more symmetric peak with a maximum shifted to higher BE values. This is indicative of the lower graphitic order of the surface of the CNFs as indicated by HRTEM (Figure 6). Furthermore, all of the CNF samples exhibit a region of high intensity between ~285 and ~291 eV, attributable to carbon heterobonds. In particular, this feature shows a long high BE tail for N-CNF873K and VGCNF, being more pronounced for the former. According to the analysis presented in Table 2, VGCNF has a higher oxygen content on the surface, whereas N-CNF873K exhibits more nitrogen. A distinct additional feature in this region, at ~288.8 eV, is observed for CNFox and is assigned to oxygen functional groups.[43,52] We therefore propose that for N-CNF873K the broader tail toward BE values below 288.8 eV is related to N−C species and not to oxygen functionalities.

A detailed analysis of the C1s region between ~285 and ~291 eV is beyond the scope of this work as the surface is highly heterogeneous. In this region, it is very difficult to deconvolve the C1s spectra, because of the many possible overlapping contributions of both oxygen and nitrogen functionalities.

4.1.2. N1s Region. Analysis of the N1s and O1s provides more detailed information on the N and O species on the carbon surface. The BE values of the most common nitrogen and oxygen species in carbon materials reported in literature are summarized in Table 4 and are compared with the values found in this work.

As suggested by theoretical calculations,[72] three different BE regions can be identified in the N1s core level spectra of carbon materials:[73] the first region between 400 and 398 eV is attributed to carbon−nitrogen bonds; the second region between 401 and 400.5 eV is attributed to nitrogen−hydrogen bonds and the third region between 403 and 406 eV to nitrogen−oxygen bonds. In detail, the region between 398 and 399 eV[53–57] is usually assigned to pyridine-like N atoms, which contribute to the π system with one p-electron (denoted as N1 for simplicity). The pyridine-like N-atom is sp^2-hybridized, with the ion-pair electrons in the sp^2 hybrid orbital that does not participate in π-system. The nonbonding (sp^2) electron is therefore easier to ionize than an electron in a π-system and hence appears in the XP spectrum at lower BE.

The region between 400 and 400.5 eV corresponds to N atoms in a pyrrole-like configuration,[53–59] donating two p-electrons to the π-system (N3 400.1 ± 0.1 eV), as is the case for both pyrrole and pyridone functionalities. The pyridone species is the tautomeric form of a lactam (the structural form reported in Figure 1) and is represented as a pyridine species with hydroxyl group in α-position to the N atom in the aromatic ring. The BE region around 2.5 eV higher than N1 is usually assigned to any form of quaternary nitrogen (N4 401.1 ± 0.1 eV),[53–59] such as quaternary N due to intra- or intermolecular hydrogen bonds between pyridine or aniline functions. This component is also assigned to the so-called substitutional "graphitic" nitrogen.[58] Substitutional N refers to N substituting a C atom in the graphitic structure, in which the nitrogen forms three σ-bonds with neighboring C or H atoms and contributes two electrons to the π-system. The proposed structure of graphitic nitrogen is reported in Figure 1. This nitrogen species carries a formal positive charge. It should be noted that the existence of this species is the subject of debate in literature.[58,74] Theoretical model calculations[75] on N substitution in graphene have shown that, with increasing N concentration, an excess of electrons originate from N and occupy the π^* antibonding states, destabilizing the planar geometry. This energy is sufficient to

(52) Wild, U.; Pfänder, N.; Schloegl, R. *Fresenius' J. Anal. Chem.* **1997**, *357* (4), 420–428.
(53) Boudou, J. P.; Chehimi, M.; Broniek, E.; Siemieniewska, T.; Bimer, J. *Carbon* **2003**, *41* (10), 1999–2007.
(54) Kapteijn, F.; Moulijn, J. A.; Matzner, S.; Boehm, H. P. *Carbon* **1999**, *37* (7), 1143–1150.
(55) Staczyk, K.; Dziembaj, R.; Piwowarska, Z.; Witkowski, S. *Carbon* **1995**, *33* (10), 1383–1392.
(56) Jansen, R. J. J.; van Bekkum, H. *Carbon* **1995**, *33* (8), 1021–1027.
(57) Pels, J. R.; Kapteijn, F.; Moulijn, J. A.; Zhu, Q.; Thomas, K. M. *Carbon* **1995**, *33* (11), 1641–1653.
(58) Buckley, A. N. *Fuel Process. Technol.* **1994**, *38*, 165–179.
(59) Kelemen, S. R.; Gorbaty, M. L.; Kwiatek, P. J. *Energy Fuels* **1994**, *8* (4), 896–906.

Table 4. Literature Assignments of the BE of the Most Common Nitrogen and Oxygen Species Present in Carbon Materials[a]

type of N	pyridine	amine	amide	pyrrole/pyridone	quarter.	N-oxide/nitro	material	ref
BE [eV]	398.3			400.1/399.5	401.3	403.1	AC	53
	398.7 ± 0.3			400.3 ± 0.3	401.4 ± 0.5	402−405	Char	54
	398.9 ± 0.1			400.9		403.1 ± 0.5	NC	26
	398.3 0.1			400.1 ± 0.1	401.3 ± 0.1	403.1 ± 0.1	Char	55
	398.7	399.9	399.9	400.7/399.7	402.5 ± 0.5		AC	56
	398.7 ± 0.3			400.4 ± 0.3	401.4 ± 0.3	402−404	Char	57
	398.6 ± 0.1	399.6		400.3	401.5		Coal	58
	398.8 ± 0.1			400.2 ± 0.1	401.4 ± 0.1	402−404	Coal	59
		400.2	399.4				CNT	60
		399.7					SWT	61
						399.7−403.1	MC	62
						400.2/406	CNT	63
	398.4 ± 0.1		399.4 ± 0.1	400.1 ± 0.1	401.1 ± 0.1	406 ± 0.1	CNF	this work

type of O	quinones	C=O	OH	C−O	NO_x	COOH	H_2O	mater.	ref
BE	530.9						533.4	CNT	44
		531		532.5			534	CF	64
		531.65−531.94		533.3−533.8				CNT	65
		531.4	533.5				533.5	ACF	66
		530.6/532.3*	534.3	532.3−533.5		534.3	536.3	AC	67
	531.1	532.3	534.2	533.3	534.3		535.9	AC	68
							533	G	69
		531.6	532.4			533.6	535−6	CF	45
		531.4−531.6	533.5	533−533.1		532.3	535.5	CF	70
		530.3		533	531.6			G	71
	530.7 ± 0.1	531.4 ± 0.1	533.7 ± 0.1	532.4 ± 0.1	533.1		535 ± 0.1	CNF	this work

[a] Acronyms: AC, activated carbon; NC, Nanocarbon; SWT, single-walled nanotubes; GF, graphite fiber; ACF, activated carbon fiber; G, graphite; MC, model compound. (*) Carbonyl in ester or amide.

change from a planar configuration to an "out of plane" bonding configuration. A natural consequence of the corrugation induced by nitrogen doping is the bending and thus rolling of the graphene cluster to form tubes. This is corroborated by experimental evidence of the effect of nitrogen insertion to induce curvature of graphene layers.[76] However, since the law of charge conservation must be observed, a counteranion, free or covalently bonded, must accompany the N atoms in this structural configuration.

It is generally accepted that, in the N1s XPS spectrum, oxidized forms of nitrogen show BE above 402 eV (see ref Table 4). Pyridine oxide (N5) is shifted ∼4.5 eV to higher BE than pyridine,[33,42,53] while a BE shift of up to 6.5 eV is observed for nitro- functionalities (N6). In fact, the N components present in Figure 4a are consistent with the literature data summarized in Table 4. The N1s XP spectra for the other samples (Figure 4b−d) are however very broad and cannot be fitted by considering only these five species. The BE region between 399 and 400 eV has been subject to less analysis in the literature and is usually assigned to functionalities containing a N−H bond in a chemical bonding state that is intermediate between a pyridine-like and a pyrrole-like configuration.

In contrast to the other N-species, there is a notable uncertainty in determining the nature of the N2 (399.5 ± 0.1 eV) species based on the XPS BE shift. Through analogy with the BE of model compounds, there are several possible species, all of which have nearly the same BE: amino groups attached to aromatic rings,[60] amide groups,[77] and nitroso groups.[62] It should be noted that this peak is located at 399.6 eV for CNFox and at 399.4 eV for the other samples (N-CNF473K, N-CNF673K, N-CNF873K). This implies that the N2 species in CNFox has a different chemical structure than in the aminated samples. Among all the samples investigated, only the CNFox sample shows a modification induced by the synchrotron beam, as is discussed in section 4.1.4.

4.1.3. O1s Region. Table 4 also shows the BE values of the most common oxygen functionalities in carbon materials reported in the literature. The chemical assignment of the components found in the analysis of the O1s is, however, controversial and no common interpretation yet exists. According to our analysis, the O1s XP spectrum can be divided into

(60) Gabriel, G.; Sauthier, G.; Fraxedas, J.; Moreno-Mañas, M.; Martínez, M. T.; Miravitlles, C.; Casabó, J. *Carbon* **2006**, *44* (10), 1891–1897.
(61) Kovtyukhova, N. I.; Mallouk, T. E. *J. Phys. Chem. B* **2005**, *109* (7), 2540–2545.
(62) Batich, C. D.; Donald, D. S. *J. Am. Chem. Soc.* **1984**, *106* (10), 2758–2761.
(63) Graupner, R.; Abraham, J.; Vencelova, A.; Seyller, T.; Hennrich, F.; Kappes, M. M.; Hirsch, A.; Ley, L. *Phys. Chem. Chem. Phys.* **2003**, *5* (24), 5472–5476.
(64) Desimoni, E.; Casella, G. I.; Morone, A.; Salvi, A. M. *Surf. Int. Anal.* **1990**, *15* (10), 627–634.
(65) Okpalugo, T. I. T.; Papakonstantinou, P.; Murphy, H.; McLaughlin, J.; Brown, N. M. D. *Carbon* **2005**, *43* (1), 153–161.
(66) Maciá-Agulló, J. A.; Cazorla-Amorós, D.; Linares-Solano, A.; Wild, U.; Su, D. S.; Schlögl, R. *Catal. Today* **2005**, *102−103*, 248–253.
(67) Walczyk, M.; Swiatkowski, A.; Pakula, M.; Biniak, S. *J. Appl. Eectrochem.* **2005**, *35* (2), 123–130.
(68) Figuereido, J. L.; Pereira, M. F. R.; Freitas, M. M. A.; Orfao, J. J. M. *Carbon* **1999**, *37* (9), 1379–1389.
(69) Marchon, B.; Carrazza, J.; Heinemann, H.; Somorjai, G. A. *Carbon* **1988**, *26* (4), 507–514.
(70) Kozlowski, C.; Sherwood, P. M. A. *J. Chem. Soc., Farad. Trans.* **1985**, *81* (11), 2745–2756.
(71) Schlögl, R.; Loose, G.; Wesemann, M. *Solid State Ionics* **1990**, *43*, 183–192.
(72) Casanovas, J.; Manel Ricart, J.; Rubio, J.; Illas, F.; Jimnez-Mateos, J. M. *J. Am. Chem. Soc.* **1996**, *118* (34), 8071–8076.
(73) Schlögl, R. In *Handbook of Heterogeneous Catalysis*, 2nd ed.; VCH: Weinheim, Germany, 2008; pp 357−427.
(74) Tucker, S. A.; Acree, W. E., Jr.; Tanga, M. J. *Appl. Spectrosc.* **1991**, *45* (7), 1188–1192.
(75) dos Santos, M. C.; Alvarez, F. *Phys. Rev. B* **1998**, *58* (20), 13918–13924.
(76) Sumpter, B. G. *Int. J. Quantum Chem.* **2009**, *109* (1), 97–118.
(77) Fustin, C. A. *Surf. Sci.* **2001**, *474* (1−3), 37–46.

the following regions (Figure 5): O1 (530.7 eV) corresponds to highly conjugated forms of carbonyl oxygen such as quinine or pyridone groups;[42,57] O2 (531.1−531.8 eV) is assigned to a carbon−oxygen double bond; O3 (532.6 eV) is a carbon−oxygen ether-like single bond; and O4 (533.5 eV) refers to carbon oxygen single-bonds in hydroxyl groups. It should be noted that the assignments of O3, O4, and O5 are not entirely unambiguous. According to Sherwood et al.,[70] the two oxygen atoms in a carboxylic acid group are equivalent with an intermediate character between single and double bond, and they give rise to the peak around 532−533 eV (O3 in this case). This fact might occur if two neighboring C−O single bond and C−O double bond are involved in tautomeric equilibrium.[70] The BE of water is also debated. Extensive studies of the adsorption of water carried out on polycrystalline graphite have led to the identification of a very broad peak centered at 533 eV.[69] Regarding the assignment of O5 (535.2 eV), some authors assign it to adsorbed water and/or oxygen. We have observed that this species is always present even upon heating and that its intensity follows the increase in the water detected by TPD-MS. It is thus quite likely to be due to the adsorption of the water formed during the thermal decomposition of surface species.

4.1.4. Influence of Functionalization Temperature. To highlight the change in the distribution of N and O species with increasing temperature of functionalization, Table 2 reports the BE and the abundance of all N and O components for the series of samples investigated.

The amount of the pyridine species (N1) is seen to increase with the functionalization temperature and it is the most abundant species for the sample functionalized at 873K. This is because, at high temperatures, aromatic cyclic moieties of nitrogen are stabilized at the edge of graphitic domains in carbon materials. In contrast, N2 is the main species when the functionalization is conducted at lower temperature (473 K). As reported in section 3.1, N insertion occurs through the reaction of NH_3 with oxygenated surface species (most likely carboxylic acid groups); therefore, it is quite probable that N is present within functionalities which also contain O. On the basis of this consideration, the N2 species in the N-CNFs might reasonably be assigned to a species in the same binding configuration as amide groups.

When the functionalization is conducted at 673 K, the N1s line shape is less well-defined, with broadening to the high BE side due to the simultaneous decrease of N2 and the increase of N3 nitrogen. The intensity of the N3 species is greatest for N-CNF673K and decreases with increasing functionalization temperature due to conversion into N1 species. The N3 species is attributed to an intermediate species such as pyridone or pyrrole groups.[33] This then results in pyridine formation upon heating. The similar O and N content in N-CNF673K suggests that nitrogen is present in functionalities accompanied by oxygen as was the case for N-CNF473K.

In the case of CNFox, N6 is the main species present in the nitrogen spectrum. This is in agreement with literature data.[53] Initial oxidation by nitric acid introduces small amounts of nitrogen in form of nitro functionalities, probably intermediate species which are subsequently transformed into oxygenated functionalities. A further very broad peak is present between 398 and 400 eV with its maximum at 399.6 eV. The exact chemical nature of this peak remains unclear; however, it is a common feature reported after nitric acid oxidation of carbon materials.[78,79] This region is usually assigned to nonoxidized nitrogen species, although some authors have reported that nitroso functionalities can also have this BE shift.[62] In this work, we observed a beam sensitivity of the N6 species, and a subsequent partial conversion from N6 into the very broad peak (in the region of the N2 species) upon exposure to the synchrotron beam for few seconds. Therefore, it is likely that the nitro species are converted into a reduced form of nitrogen due to irradiation by X-rays, thereby causing a chemical shift as described above. Simultaneously, a decreased intensity at 533.1 eV is observed in the O1s assigned to the oxygen−nitrogen bond.

Considering N-CNF873K, as reported in Table 2, the small amount of O2 (oxygen−carbon double-bound) or O4 (oxygen−carbon single-bond) with respect to the amount of the N3 component (nitrogen in pyridone or pyrrole species), suggests that for this sample the N3 species is also due to pyrrole groups. Note that different chemical structures may have the same chemical shift and contribute to the same XP peak.

The amination process, in general, produces a strong decrease in the absolute abundance of the carbon−oxygen single-bond in hydroxyl groups (O4) and in ether-like oxygen (O3). This reflects a change in the character of the surface from predominantly hydrophilic in CNFox and N-CNF473K toward a more hydrophobic nature in N-CNF673K and N-CNF873K.

4.1.5. Summary. On the basis of the results presented herein, it is experimentally justified to introduce several components in the deconvolution of the XPS spectra. The XPS chemical shift analysis cannot always be straightforwardly assigned to a specific chemical structure; however, it still provides important information for evaluating the chemical nature of the species generating the signal.

The data demonstrate that the amination of CNFs is possible through defect-group derivatization, the defects being predominately carboxylic oxygen species. This contrasts with the amination pathway reported for fullerene which occurs via direct covalent sidewall derivatization.[25] The latter reaction pathway is more favorable in fullerene due to the presence of pentagons/heptagons, which cause curvature of the planar graphene layer, increase the bond strain and render the fullerene reactive toward amination.[80] This eliminates the need to first introduce defects in the graphitic structure as is required in the case of the CNFs investigated herein.

The concentration of N and O species is temperature dependent, as shown in Table 3. In the case of the oxygen species, the thermal stability of the functional groups determines the amount of oxygen present at the surface; thus, the higher the treatment temperature, the lower the amount of O species present. The quantity of N inserted is dependent upon two competitive reactions: the reaction of NH_3 with the oxygen species at the CNF surface, and the thermal decomposition of the oxygen species.

XPS analysis has shown that the distribution of the different species is affected by the treatment temperature in a trend that follows the pathway of nitrogen insertion already reported in literature[33,57,81] and depicted here in Figure 16. During the initial

(78) Yang, C.; Kim, D. Y.; Lee, Y. H. *Chem. Mater.* **2005**, *17* (25), 6422–6429.
(79) Pietrzak, R.; Wachowska, H. *Fuel Process. Technol.* **2006**, *87* (11), 1021–1029.
(80) Lin, T.; Zhang, W.-D.; Huang, J.; He, C. *J. Phys. Chem. B* **2005**, *109* (28), 13755–13760.
(81) Jansen, R. J. J.; van Bekkum, H. *Carbon* **1994**, *32* (8), 1507–1516.

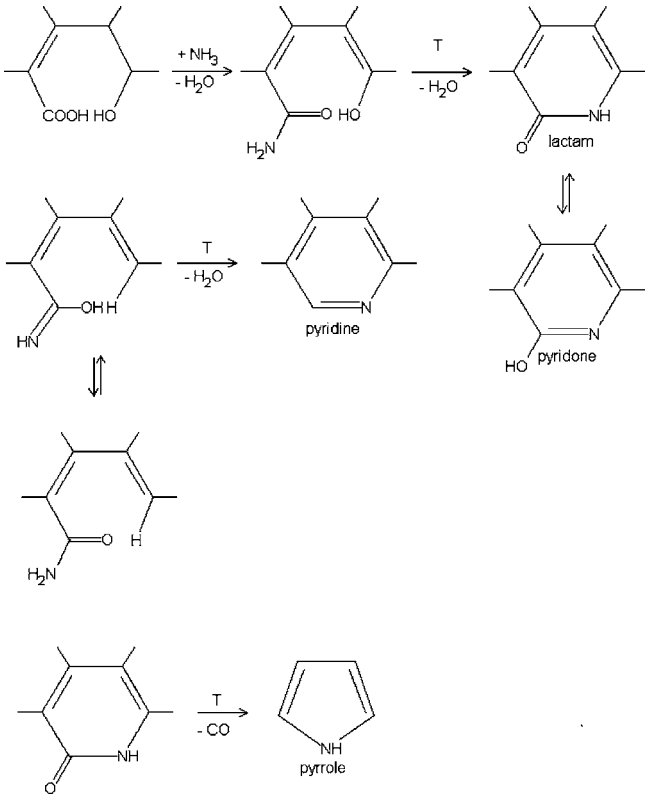

Figure 16. N insertion pathway in carbon.

stages of heating, NH_3 reacts with carboxylic acid species present on the carbon surface to form intermediate, possibly amide-like, species. At functionalization temperatures between 473 and 673 K, the introduced nitrogen tends to be present in functionalities which also contain oxygen, with higher temperatures increasing the amount of N inserted. Depending on the final treatment temperature, those species undergo dehydration (e.g., pyridone and pyridine) or decarbonylation (e.g., pyrrole) reactions to form more stable heterocyclic aromatic moieties. Increasing the functionalization temperature to 873 K results in competitive NH_3 thermal decomposition and surface oxygen species decomposition becoming more favored, thereby leading to a decrease in the overall N content. At higher temperatures, the defect-containing graphene layers have sufficient energy to undergo rearrangement and remove the defects such that the most thermodynamically stable structure is formed. This is also a reason why it is more difficult to introduce larger amount of N species at higher temperature. Removal of the O atoms in the graphitic-like structure occurs in a more pronounced manner than for the N atoms.

4.2. Surface Chemical Properties. The assignment of the XP spectra, as discussed in section 4.1, allows for a description of the surface functionalities present after amination. When combined with liquid-phase titration, zeta potential, and microcalorimetry measurements, a complete description of the surface properties of the functionalized NCs is obtained.

An important parameter in the application of N-NCs is their surface basicity. This influences, in particular, the adsorption behavior of such materials. In early XPS studies by Shirley,[82,83]

Table 5. Summary of Basic Sites Potentiometric Titration and CO_2 Microcalorimetry Adsorption Results of the N-CNFs Samples

	liquid phase titration		gas phase microcalorimetry	
sample	mol basic site/g	pK_a	amount of CO_2 (monolayer) mol/g	initial differential heat of adsorption kJ mol^{-1}
N-CNF473K	4.5×10^{-4}	7,9; 7.8	5×10^{-6}	90
N-CNF673K	6×10^{-4}	8.2; 8	1.5×10^{-6}	50
N-CNF873K	1×10^{-3}	8.35; 8.34	8×10^{-6}	150

the correlation between the variation in proton affinity and the corresponding variation in the O1s and N1s BE was investigated for a series of alcohols and amines. Accordingly, for a series of alkyl-substituted aliphatic amines or alcohols, the final state polarization effects determine the chemical shift in such way that the greater the stabilization of the photoemission induced charge on the O or N by the surrounding groups then the more pronounced the BE shift to a lower value becomes. This concept can be applied to the present work by considering the BE shift as a measure of the Brønsted basicity of the functional groups present on the aminated CNFs. Thus, samples with a higher amount of those species at lower BE in the XP spectra are expected to show higher basicity. As such, the pyridine species observed in the N1s XP spectra should be the most basic species. The number and strength of basic sites has also been probed by liquid-phase titration and gas-phase microcalorimetry. A summary of these data is presented in Table 5. Liquid-phase titration of the basic sites has shown that their strength and number increase slightly with increasing the functionalization temperature. This seems to be in contradiction with expectations based on the total amount of nitrogen detected by XPS or by elemental analysis (Table 3). However, it is important to consider that, during the equilibration time that precedes the titration, the acidic species on the carbon surface may already have neutralized the basic species present. For instance, since the sample functionalized at 473 K still contains oxygen functionalities with acidic character, the total volume of acid added is lower as compared to the higher temperature functionalized samples which do not contain such sites. The distribution in strength of nitrogen and oxygen basic and acidic sites varies across the entire set of samples investigated. The calculated pK_a values range from 7.9 to 8.35 and show slight scatter as a consequence of the presence of a different distribution of acidic and basic species, as determined by XPS analysis. It is interesting to note that the volume of titrant added to the first EQP increases with the functionalization temperature. This is similar to the increasing amount of the pyridine species (which is theoretically the most basic species) observed in the N1s XPS. Table S1 (Supporting Information) reports pK_a values for the most common organic base compounds. It can be seen that the values obtained for N-NCs in this work are closer to the values reported for aliphatic amines than to the value reported for pyridine (pK_a 5.2). The presence of O basic sites should also be considered, thereby influencing the acid/base character of the carbon surface.[84] Theoretical calculations by Montes-Morán[84] have highlighted that the pK_a value of certain species substituted in the benzene ring is influenced by the number of poly-condensed aromatic cycles, the bonding configuration of the species and their mutual position within the cluster. Additionally, basal planes of graphene are considered binding

(82) Shirley, D. A. *J. Electron Spectrosc. Relat. Phenom.* **1974**, *5* (1), 135–148.
(83) Martin, R. L.; Shirley, D. A. *J. Am. Chem. Soc.* **1974**, *96* (17), 5299–5304.
(84) Montes-Morán, M. A.; Suárez, D.; Menéndez, J. A.; Fuente, E. *Carbon* **2004**, *42* (7), 1219–1225.

sites for protons in their own right. The basic strength of these basal planes, however, appears to be much lower than the most basic poly-condensed aromatic cycles species proposed in literature.[84] On the basis of these finding, the authors assign the basic character of the carbon surface to γ-pyrone-type species which are considered to be a combination of non-neighboring carbonyl (sp^2) and ether (sp^3) oxygen species at the edge of poly-condensed aromatic clusters. The main reason for the basicity of pyrone-like structures is the stabilization of the protonated form via the electronic π-conjugation throughout the sp^2 system. According to this study, this occurs most readily for O- and to a lesser extent for highly conjugated N-species. In contrast to the reported theoretical calculations,[84] it is well-known from experiments that N-containing carbon materials have increased acid adsorption capacity when compared to thermally treated oxygenated carbon materials.[85] Therefore, further investigations are required in order to clarify the structure of the basic species present in nitrogen-containing carbon materials.

Microcalorimetry experiments reveal additional insights as to the nature of the adsorption sites present on the surface of the CNFs. Further to the results presented in section 3.2, the differential heat of adsorption in the monolayer region as function of CO_2 uptake for the various samples is shown in Figure 13. The highest value of the differential heat of adsorption, estimated from the first adsorption point, was measured for the sample N-CNF873K and is $\sim$150 kJ mol^{-1}. In the case of N-CNF873K, after the desorption process, readsorption results in a lower differential heat (Figure 13a) which is indicative of the fact that some very strong basic sites are lost during the first adsorption run. The value of the initial differential heat of adsorption for the second run approaches the value found for N-CNF473K (90 kJ mol^{-1} in Figure 13b). A similar value of differential heat of adsorption is reported in the literature[86] for amino groups grafted onto SBA-15. At high coverage the curve of the heat of adsorption for N-CNF473K almost coincides with that of N-CNF873K. In this case, the formation of a monolayer therefore also takes place. N-CNF673K gives rise to a heat of adsorption of $\sim$50 kJ mol^{-1}. In contrast to N-CNF873K, however, in this sample, the secondary reaction occurs before the monolayer is formed. In fact, the value of the differential heat of adsorption oscillates with increasing coverage but never reaches the value of the heat of CO_2 condensation. It is interesting to note that the heat of adsorption measured for the commercial VGCNF is very low at around 30 kJ mol^{-1}; however, it is slightly above the enthalpy of liquefaction of carbon dioxide (ΔH_{liq} 17 kJ mol^{-1}).[87,88] There is therefore a moderate interaction between the adsorbed carbon dioxide molecules and the VGCNF surface. Secondary reactions also occur on this sample, although in this case they take place before the formation of a monolayer (the heat of adsorption increases without reaching the value of the enthalpy of liquefaction of CO_2).

In the most basic sample (N-CNF873K), microcalorimetry measurements provide evidence of a few very strong basic sites which coexist with the majority of the sites which are weakly basic. Both microcalorimetry and potentiometric titration indicate that this is the most basic sample. A disparity occurs however when comparing microcalorimetry and titration data for N-CNF673K. According to microcalorimetry, this sample contains the lowest amount and weakest basic sites; however, potentiometric titration indicated a larger amount of basic sites than for N-CNF473K. This difference is due to the differing analytical procedures. For potentiometric titration, the sample is in an aqueous suspension. The higher number of basic sites apparent is due to the dynamic character of the carbon surface, which may undergo changes during the measurement. For instance, the lactam species, which are the most abundant on N-CNF673K, can undergo bond hydrolysis in water, leading to the higher amount of basic sites determined by potentiometric titration. It is also important to remember however that, as was mentioned in section 3.2, the secondary processes before the formation of the monolayer observed by microcalorimetry hinder the exact determination of the distribution of basic site strengths in this sample. This can be understood if, in this case, the adsorption sites undergo a change through the formation of an intermediate species (e.g., through bond cleavage), which reacts with CO_2 thereby hindering the determination of the basic strength distribution. Because of the presence of the irreversible secondary processes, the observed differential heat could be the result of subsequent endothermic and exothermic processes and thus not representative of the strength of the basic sites.

The secondary processes observed by microcalorimetry may include the reaction of CO_2 with surface species, for example, phenol or nitrogen species forming carbonate[89] and carbamate,[90] respectively. As reported by kinetic studies,[89] carbamate formation occurs with fast kinetics on aliphatic amines, while on aromatic nitrogen containing molecules, the reaction is slower due to the disruption of the π-conjugation. This is in agreement with our result showing that secondary processes occur at a lower dosing pressure for N-CNF673K and N-CNF473K which contain the most abundant N species with N in sp^3 configuration, and only at higher dosing pressures for N-CNF873K, which contains N in mainly sp^2 configuration. In addition, it cannot be excluded that the species formed as consequence of the interaction of CO_2 with the surface functional groups undergo decomposition, with an equimolecular release in the gas phase of secondary species. This would contribute to the pressure in microcalorimetry chamber and hinder the exact quantification of the basic sites. Such a process would explain the low amount of adsorbed CO_2 observed in the isotherms for N-CNF673K and N-CNF473K.

For N-CNF873K, the quantity of basic sites measured in the isotherm of the readsorption step is the same as in the first adsorption process. Readsorption may occur on the same number of (now modified) basic sites as during the first run of CO_2 adsorption. Another possible explanation is that the secondary reaction occurring at higher CO_2 coverage leads to the irreversible conversion of the very strong basic sites (i.e., formation of carbonate species). The readsorption of CO_2 on the same sample leads to a lowering of the differential heat of adsorption similar to the differential heat of adsorption measured for the sample N-CNF473K. This value was reported for N group grafted on

(85) Boehm, H. P. In *Carbon Materials for Catalysis*; Serp, P. , Figueiredo, J. L. , Eds.; WILEY_VCH: Hoboken, NJ, 2009; pp 219−265.
(86) Knöfel, C.; Descarpentries, J.; Benzaouia, A.; Zeleòàk, V.; Mornet, S.; Llewellyn, P. L.; Hornebecq, V. *Microporous Mesoporous Mater.* **2007**, *99* (1−2), 79–85.
(87) Winter, W.; Xia, X.; Hereijgers, B. P. C.; Bitter, J. H.; van Dillen, A. J.; Muhler, M.; de Jong, K. P. *J. Phys. Chem. B* **2006**, *110* (18), 9211–9218.
(88) Shen, J.; Cortright, R. D.; Chen, Y.; Dumesic, J. A. *Catal. Lett.* **1994**, *26* (3−4), 247–257.
(89) Caplow, M. *J. Am. Chem. Soc.* **1968**, *90* (24), 6795–6803.
(90) Goettmann, F.; Thomas, A.; Antonietti, M. *Angew. Chem., Int. Ed* **2007**, *46* (15), 2717–2720.

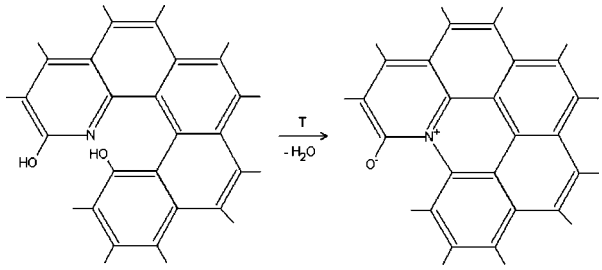

Figure 17. Pathway for the formation of a hypothetical structure of quaternary N.

SBA-15,[86] which suggest that in the second readsorption run the N basic sites are probed.

The adsorption isotherms of N-CNF473K and N-CNF873K have been analyzed and are seen to fit well to the Langmuir adsorption model, with an order greater than one. This fact confirms that this is not a pure adsorption process but instead that secondary reactions contribute to the differential heat of adsorption. This is especially apparent in Figure 13b for N-CNF473K (blue spots) where the differential heat of adsorption increases drastically at 5 μmol g^{-1} of adsorbed CO_2. At this point, 30 kJ mol^{-1} of the differential heat is due to the pure adsorption and 40 kJ mol^{-1} is due to the secondary processes. On the basis of these results, a hypothetical structure of the strongest basic sites can be assumed.

In particular, in a pyrone-like structure where both O and N species are present, due to the different electronegativity between the O and N atoms, the charge accumulation is expected on the O atom rather than on the N atom. Such a structure may easily occurs on the sample N-CNF873K. For instance, the conversion via the condensation of pyridone and the adjacent phenol leads to the formation of a zwitterionic structure, containing a relatively strong basic site (anionic oxygen in Figure 17). Such a structure has a pK_a similar to phenol (pK_a 8−11). This assumption would justify the existence of the high thermal stable quaternary nitrogen (N4 in N1s for N-CNF873K Figure 4a). Such a species could be responsible of the high differential heat of CO_2 adsorption measured for the samples N-CNF873K by microcalorimetry (section 3.2.2). This value is comparable to the differential heat released by the adsorption of CO_2 on the oxygen basic sites in hydrotalcite[87] and γ-Al_2O_3.[88]

XPS, microcalorimetry, and potentiometric titration data have therefore provided a clearer picture of the nature of the surface species present on CNFs after amination. In particular, insights into the strength, number, and chemical structure of the basic presents have been garnered.

4.3. Electronic and Bulk Structure. Techniques such as XPS have been used to probe the surface structure of the CNFs. However, as indicated through a comparison of hot-gas extraction and XPS data in section 3.2.1 (Table 3), the surface and bulk structure of the materials can be very different, with the bulk properties playing a key role in applications such as composite materials. Of particular interest is the electronic character of the materials before and after functionalization.

C1s XPS has shown the modification of the electronic structure induced by the different functionalization treatments. The tail in the high energy side to the C1s between 285 and 291 eV, which was more pronounced for N-CNF873K than for CNFox and pristine VGCNFs, is indicative of the presence of localized charge accumulation on the defect sites, that is, the heteroatom, producing the shift to higher BE of the photoemitting carbon atom bound to the heteroatom. Some of the electronic states behave as basic sites as determined by the liquid phase titration and microcalorimetry. The introduction of highly electronegative oxygen species in CNFox through oxidative treatment, appearing as a well-defined peak at 288.8 eV in the C1s XP spectrum, leads to the carbon surface taking on acidic character in aqueous solution.

THz-TDS measurements have also been conducted in order to probe the electronic effects of amination. As is clear from Figure 15, there are some notable differences in the terahertz characteristics of the CNF before and after functionalization. To quantify these differences, the spectra have been modeled using a Drude-Lorentz (DL) model and employing an effective medium approximation (EMA). Rough fits were obtained which suggested that the unfunctionalized sample had a slightly higher density of free electrons, and consequently fewer defect sites when compared to the N-functionalized sample. This is despite the higher absorption coefficient for the N-functionalized sample, which has previously been qualitatively correlated with electron density. However, the lower refractive index offsets this difference. It should be noted that these results are not conclusive, but only give an indication of the underlying electronic characteristics of the material, especially given the unknown differences that may have been incorporated into the structure as a result of the functionalization. However, it is clear that despite the disruption to long-range graphitic order the free electron density and conductivity remains very similar after functionalization. This can tentatively be explained as evidence of a greater local electron density around specific sites in the functionalized material. This is consistent with the hypothesis of electronic modification being localized around N and O atoms. It is also notable that HRTEM (Figure 6) did not identify significant differences in the long-range structure of the CNF after functionalization. This is a consequence of the localization of functionalization on the CNF surface, evidenced by comparing the surface and bulk composition of the sample through XPS and hot-gas extraction measurements (Table 3). It should be noted that this is the first report of THz-TDS of N-functionalized NCs and further studies will be necessary before a complete understanding of such systems can be developed.

The bulk structure of the materials, and their electronic landscape, appears to be relatively unaffected by functionalization as compared to their surface structure. This is because of the local nature of the N-functionalization and the localized charge accumulation around these N-sites.

5. Conclusions

N-containing CNFs were prepared via postsynthesis functionalization with NH_3. The distribution of N and O species as a function of temperature has been determined through the use of a variety of complementary techniques probing both the surface and bulk electronic properties of the materials. It was found that the presence of oxygen-containing functionalities is a prerequisite for introducing a high amount of nitrogen-containing moieties onto the CNFs surface. The samples are characterized by the coexistence of acidic and basic N and O species. The temperature of the functionalization treatment influences the population of O and N species and thus affects the acidic and basic properties and hydrophobic/hydrophilic character of the carbon surface. Heterogeneously distributed and energetically different (basic) adsorption sites are present on the surface of the functionalized CNFs depending on the treatment temperature. At 473 K, nitrogen moieties are introduced as consequence of the reaction of carboxylic acid sites

with NH_3 and appear in the XP N1s spectra as the main N2 species with BE at 399.6 eV (sample N-CNF473K). Although the nature of this species could not be unequivocally determined here, the coexistence of a corresponding amount of O in this sample suggests that these species might be N species accompanied by O, for example, in an amide-like configuration. This therefore creates a bifunctional material with both acidic and basic site on a hydrophilic surface. Increasing the functionalization temperature to 673 K results in condensation of the N2 species giving arise to heterocyclic moieties that appear as the N3 species (400.1 eV) in the XP N1s spectrum. The heterocyclic nature of this species is confirmed by the hydrophobic character of the surface for this sample. Considering that, in this case the amount of O is also relatively high, the N3 contribution in the N1s spectrum is in part related to lactam species (pyridone). Functionalization at 873 K results in a material containing very strong basic sites (150 kJ mol^{-1}) among a majority of weaker basic sites. The N species created are mainly heterocyclic moieties (pyridine-like and pyrrole-like species) which lead to a surface with hydrophobic character. While the increase in basicity was in part correlated with the amount of pyridine-like species, oxygen species in a pyrone structure containing a quaternary N atom in the adjacent fused ring may also strongly contribute to the overall basicity of the sample. Additionally, we have been able to shed the light on the existence, nature, and possible formation pathway of the aromatic "quaternary amine" of N-functionalized carbon materials. Such species are formed from the intermolecular condensation of pyridone species with phenol species and thus are more numerous in the sample functionalized at 873K. The procedure we present in this work allows, to a certain extent, the surface chemistry to be tailored; for instance, changing from a highly hydrophilic surface after functionalization at low temperature to a hydrophobic surface after preparation at higher temperature. The versatility of this functionalization route allows for applications in a variety of processes. The amide moieties introduced at 473 K may be exploited as anchoring site for the development of supramolecular systems, while the strong basic sites introduced at high temperature will alter the adsorption properties for applications in, for example, catalysis. It is expected that this synthesis procedure could be applied to other nanocarbon materials such as CNTs, graphene nanoscrolls, and so forth.

Acknowledgment. The author would like to acknowledge IMPRS for Ph.D. fellowship. Dr. Bernt Kubias, Dr. J. P. Tessonnier, Dr. D. Rosenthal, Dr. O. Timpfe are acknowledged for helpful discussion. Dr. J. Amadou is acknowledged for performing ZP measurement. Dr. S.-P. Oei and Dr. H. E. Unalan are acknowledged for deposition of CNF films to facilitate THz-TDS measurements. The reviewers are heartily acknowledged for the accurate work of reviewing and the relevant suggestions offered which improved the quality of the paper.

Supporting Information Available: Difference of the C1s spectra of CNF samples with the C1s spectra of HOPG; dissociation constants of the conjugated acid of base molecules in aqueous solution at 298 K. This material is available free of charge via the Internet at http://pubs.acs.org.

JA910169V